Journal of Alloys and Compounds 480 (2009) 617–624

Contents lists available at ScienceDirect

Journal of Alloys and Compounds

journal homepage: www.elsevier.com/locate/jallcom

Microstructural, thermal and magnetic properties of amorphous/nanocrystalline FeCrMnN alloys prepared by mechanical alloying and subsequent heat treatment

R. Amini [a,c,*], H. Shokrollahi [b], E. Salahinejad [a], M.J. Hadianfard [a], M. Marasi [a], T. Sritharan [c]

[a] Department of Materials Science and Engineering, School of Engineering, Shiraz University, Zand Blvd, 7134851154, Shiraz, Iran
[b] Department of Materials Science and Engineering, Shiraz University of Technology, Modarres Blvd, 3619995161, Shiraz, Iran
[c] School of Materials Science and Engineering, Nanyang Technological University, Block N4.1, 50 Nanyang Avenue, 639798, Singapore

ARTICLE INFO

Article history:
Received 12 November 2008
Received in revised form 22 January 2009
Accepted 30 January 2009
Available online 10 February 2009

Keywords:
Amorphous FeCrMnN alloys
Mechanical alloying
Glass transition
Crystallization
Magnetic properties

ABSTRACT

Amorphous FeCrMnN alloys were synthesized by mechanical alloying (MA) of the elemental powder mixtures under a nitrogen gas atmosphere. The phase identification and structural properties, morphological evolution, thermal behavior and magnetic properties of the mechanically alloyed powders were evaluated by X-ray powder diffraction (XRD), scanning electron microscopy (SEM), differential scanning calorimetry (DSC) and vibrating sample magnetometer (VSM), respectively. According to the results, at the low milling times the structure consists of the nanocrystalline ferrite and austenite phases. By progression of the MA process, the quantity and homogeneity of the amorphous phase increase. At sufficiently high milling times (>120 h), the XRD pattern becomes halo, indicating complete amorphization. The results also show that the amorphous powders exhibit a wide supercooled liquid region. The crystallization of the amorphous phase occurs during the heating cycle in the DSC equipment and the amorphous phase is transformed into the crystalline compounds containing ferrite, CrN and Cr_2N. The magnetic studies reveal that the magnetic coercivity increases and then decreases. Also, the saturation magnetization decreases with the milling time and after the completion of the amorphization process (>120 h), the material shows a paramagnetic behavior. Although the magnetic behavior does not considerably change by heating the amorphous powders up to the crystallization temperature via DSC equipment, the material depicts a considerable saturation magnetization after the transformation of the amorphous phase to the nanocrystalline compounds.

1. Introduction

Recently, there has been considerable interest in synthesizing the amorphous materials to obtain superior properties. The amorphous alloys with large glass-formation abilities are a novel class of engineering materials due to their exceptional mechanical properties and relatively high corrosion resistance [1–3]. This new type of materials allows for the production of stress-free amorphous and/or nanocrystalline alloys by using appropriate heat treatment methods. Furthermore, the large-scale bulk amorphous materials can be produced through powder metallurgy route and subsequent consolidation [2–5].

Although the majority of amorphous alloys are conventionally produced by the rapid solidification method, the mechanical alloying (MA) technique is a promising alternative method to synthesize these alloys [2–10]. Based on the energy of the milling process and the thermodynamic properties of the constituent elements, the alloy can be rendered amorphous by this processing [11]. Nevertheless, the MA process has normally been performed under an inert gas atmosphere like argon; the processing under a reactive gas atmosphere, such as nitrogen has been employed to produce an amorphous phase [12–16] and nanocrystalline compounds [17–21] through the solid–gas reaction.

One of the most important advanced materials which can be produced by the MA method is multi-component FeCrMnN alloys. These alloys are a new class of engineering materials with superior mechanical properties and suitable corrosion resistance [21–25], which can, both, be improved significantly by the progression of an amorphous phase in the structure. For some potential applications, such as those of biomaterials, it is necessary to use a stainless steel alloy which has a negligible response to electromagnetic fields. On the contrary, ferromagnetic properties are essential for some other applications like low-loss transformer core materials. Since magnetic properties can be influenced by the microstructure of the alloys, it is possible to produce the alloys with different structure and consequently different magnetic properties. There exist

* Corresponding author at: Department of Materials Science and Engineering, School of Engineering, Shiraz University, Zand Blvd, 7134851154, Shiraz, Iran. Tel.: +98 917 714 8204.
E-mail address: ramini2002@gmail.com (R. Amini).

0925-8388/$ – see front matter © 2009 Elsevier B.V. All rights reserved.
doi:10.1016/j.jallcom.2009.01.132

Table 1
Chemical composition of the as-milled powders.

Milling time (h)	Weight percent (wt.%)				
	Fe	Cr	Mn	N	O
24	69.12	17.98	11.91	0.71	0.28
48	68.46	17.87	11.77	1.63	0.27
72	67.85	17.74	11.69	2.42	0.30
96	66.93	17.71	11.56	3.51	0.29
120	66.30	17.69	11.61	4.12	0.28
144	66.22	17.64	11.55	4.31	0.28

several reports in the literature about the effect of milling process and/or subsequent annealing on the microstructure and magnetic properties of Fe-based alloys, for example Refs. [26–33]. Concerning stainless steels, it seems that more systematic work is required to be conducted to expand the application of these new materials. This paper investigates the formation of amorphous FeCrMnN alloys with paramagnetic properties as well as the formation of nanocrystalline FeCrMnN alloys with a ferromagnetic behavior during MA and subsequent heat treatment processes.

2. Experimental procedure

In this study, high-nitrogen Fe18Cr12Mn alloys were synthesized by the milling of pure elemental Fe (Merck, >99.5%, $D_{a.v.}$ = 50 μm), Cr (Merck, >99.9%, $D_{a.v.}$ = 150 μm) and Mn (Merck, >99.9%, $D_{a.v.}$ = 50 μm) powders under a pressurized nitrogen gas atmosphere. MA was conducted in a planetary ball mill (Fritsch, Pulverisette 5) with the tempered steel bowl (capacity = 250 ml) and balls (d = 8 mm). A rotation speed of 250 rpm and the ball-to-powder mass ratio of 30:1 was used for this purpose. The sampling of the powders was performed at 24-hour intervals.

The chemical composition of the as-milled powders was determined by using an X-ray fluorescence analyzer (XRF, PHILIPS, PW2400) and a LECO TC 436 (LECO Corp., St. Joseph, MI). In the XRF test, the quantitative values were extracted by the PAN analytical software. The morphological change of the powder particles was studied by a scanning electron microscopy (SEM, JEOL-JSM 5310). Also, the phase constituent and structural properties of the powders were investigated by using powder X-ray diffraction (XRD, SHIMADZU Lab X-6000, Cu Kα radiation). For all investigations, the angular range (2θ) of 30–100° with a step width of 0.02 and a step time of 3 s was used. The X-ray tube was operated at 40 kV and 40 mA. The quantitative analysis of the XRD data was performed by TOPAS 3 from Bruker AXS. The thermal stability of the amorphous powders was evaluated using a differential scanning calorimetry (DTA/DSC, NETZSCH, STA 449C Jupiter) with an alumina container under a flowing purified argon gas. Finally, the effect of the milling time and heat treatment on the magnetic properties of the alloyed powders was considered by a vibrating sample magnetometer (VSM, LAKESHORE 7404).

3. Results and discussion

3.1. Chemical composition

Table 1 lists the chemical composition of the samples as a function of the milling time. As it can be seen, the nominal composition of Fe18Cr12Mn was achieved. However, due to the natural oxidation of the powders, a small amount of oxygen impurity is observed in the composition. By further consideration of the results, it can be observed that the total nitrogen content steadily increases with increasing the milling time reaching 4.31 wt% at 144 h. It reveals that during milling under the nitrogen atmosphere, due to the solid–gas reactions, the high quantity of nitrogen atoms diffuses into the structure of the powders.

3.2. Microstructural studies

3.2.1. XRD analysis

Fig. 1 shows the XRD patterns of the as-milled powders at the proper stages of the milling process. As it appears, after 24 h of milling the alloying process is completed and the peaks related to the initial elements disappear. At this stage, the XRD pattern consists of the major peaks of the crystalline ferrite and austenite phases. By further progression of the MA process, due to a decrease in the crystallite size, an increase in the lattice strain and/or the existence of a considerable amount of amorphous phase in the structure, the broadening of the XRD peaks is increased. At sufficiently high milling times (higher than 96 h), the Bragg peaks related to higher-order reflections begin to disappear and the peak related to the first-order maxima becomes significantly broad. By further continuation of milling, due to the existence of a high amount of amorphous phase in the structure, the XRD pattern becomes halo. This process can be discussed as follows.

During MA under the nitrogen gas atmosphere, nitrogen can be adsorbed on the newly created surfaces of the powder particles and penetrates into the structure. The incorporation of the nitrogen atoms apparently leads to the expansion of the lattice and the

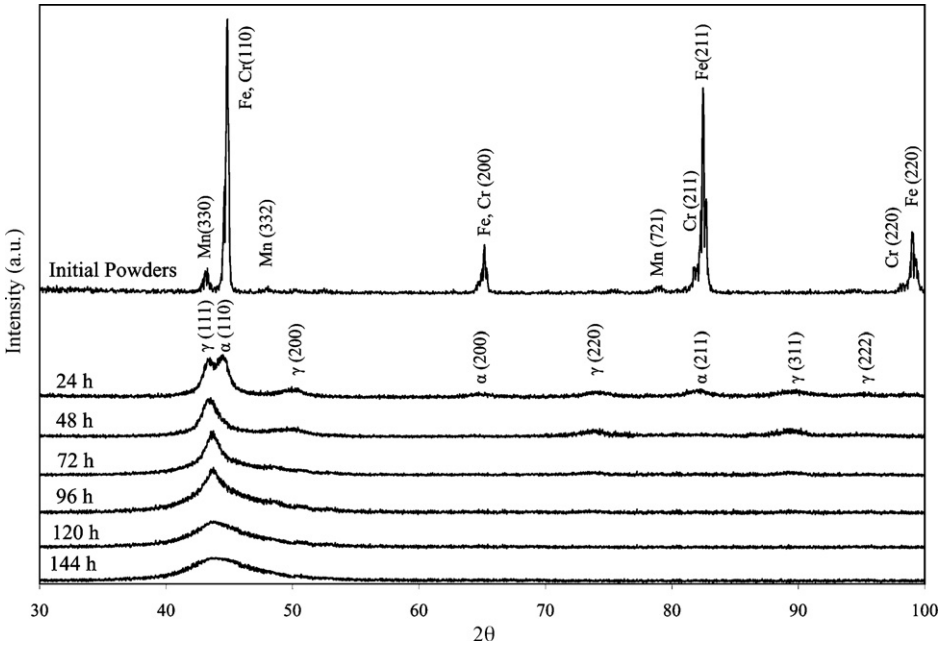

Fig. 1. XRD patterns of the as-milled powders.

Table 2
Lattice parameter, crystallite size, and lattice strain of the crystalline phases.

Milling time (h)	Lattice parameter (Å)		Crystallite size (nm)		Lattice strain (pct)	
	Ferrite	Austenite	Ferrite	Austenite	Ferrite	Austenite
24	2.8811	3.6131	21	17	0.25	0.23
48	2.8887	3.6185	14	11	0.38	0.25
72	2.8925	3.6223	11	9	0.45	0.27
96	2.8968	3.6305	10	8	0.49	0.28

increase of strain in the crystallites. In order to reduce the strain energy, a high quantity of nitrogen atoms will be segregated into the dislocations and grain boundaries and will fix them [12]. This can prevent the grain growth phenomenon, leading to the progressive grain refinement during MA. Afterwards the dropping down of the running dislocations on the fixed dislocations leads to the nucleation of new boundaries, thereby providing a nanometer structure with a crystallite size in the order of a few nanometers [34]. At a very small grain sizes (possibly less than 5 nm) and a sufficiently high concentration of nitrogen atoms, due to an increase in the constraints of the neighboring grains and the strain energy, the crystallite becomes unstable [12,13]. As the strain energy in the amorphous phase is less than the grain boundary, the amorphous phase, which is more stable than the grain boundary, will nucleate along the grain boundaries and will consume the crystalline lattice. In addition to the aforementioned reasons for the amorphization process, the intermixing at the atomic levels is another cause of the amorphization. It was reported that the intermixing of the constituent elements of iron and nitrogen does not fully occur on an atomic scale during MA and the presence of other constituents like chromium and manganese is essential to obtain a fully amorphized structure [6]. Accordingly, it seems that when Cr and Mn with a high affinity for N are added to Fe–N alloys, the intermixing of the atomic species Fe, Cr, Mn, and N readily occurs at an atomic level, resulting in the formation of an amorphous phase. Alternatively, due to the strong interaction between these atoms and N, the atomic diffusivity decreases, thereby prohibiting the diffusion of the atoms over a large distance during MA. This retards the nucleation and growth of crystallites, thereby developing the amorphization reaction in the MA process [6]. More details about the effect of nitrogen on the amorphization process during MA was reported in other works of the present authors [35,36]. In these two works, the effect of the milling atmosphere on the amorphization was considered by comparing the microstructure of the samples milled under the nitrogen and argon atmospheres.

Table 2 lists the effect of the milling time on the lattice parameter, crystallite size, and lattice strain of the ferrite and austenite phases. After 96 h of milling, due to the existence of a high amount of the amorphous phase in the structure, the major peaks of the crystalline phases (which may exist in small amounts within the amorphous matrix) disappear into the halo pattern. Consequently, the measurement of the parameters after 96 h of milling is not possible. According to Table 2, due to the continuous dissolution of nitrogen atoms into the interstitial sites of the crystalline phases and consequently the expansion of the lattice, the quantity of lattice parameter increases by increasing the milling time. Furthermore, due to the severe plastic deformation and mismatch strains of the dissolved nitrogen atoms, the lattice strain increases considerably by progression of MA. Also, the results show that the crystallite size is in the nanometric levels and decreases with increasing the milling time. This is attributed to the generation of the high density of dislocation and the segregation of infused nitrogen atoms into the dislocations and the grain boundaries during MA. More details about the variation of the aforementioned parameters with milling time were discussed in the previous paper [35].

3.2.2. SEM observations

During the mechanical milling process, the powder particles are repeatedly flattened, cold welded, fractured and rewelded [11]. Fig. 2 shows the SEM micrograph of the as-milled powder mixtures for the various milling time. The irregular nature of the powder particles is obvious in the low milling times; however, in the higher

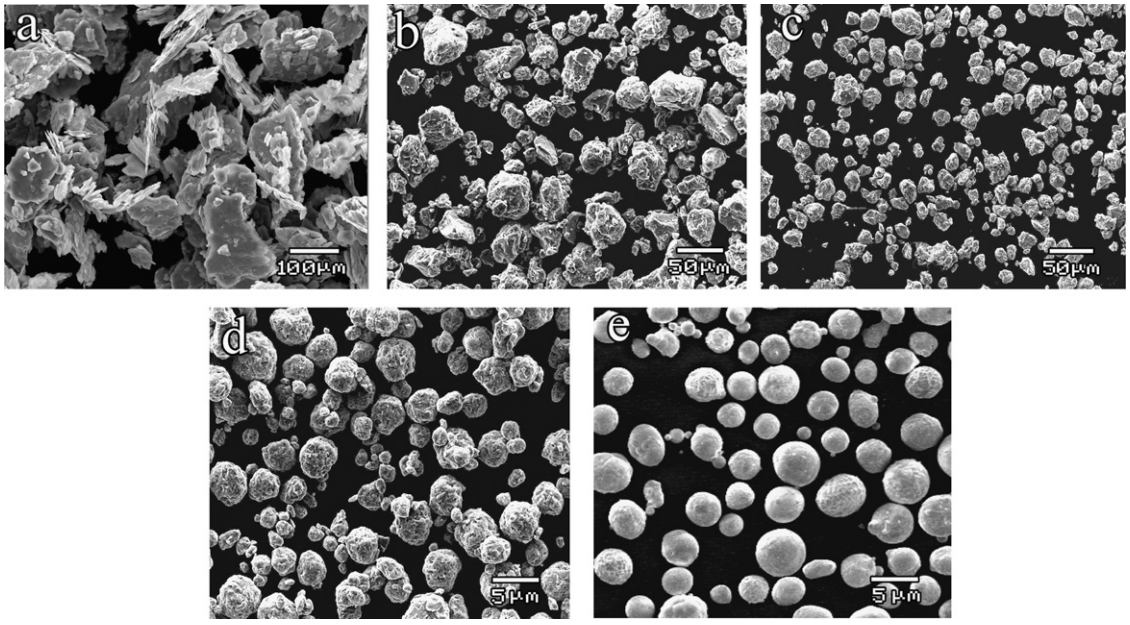

Fig. 2. Morphological changes of the as-milled powders as a function of the milling time (a) 6 h; (b) 24 h; (c) 48 h; (d) 96 h; (e) 144 h.

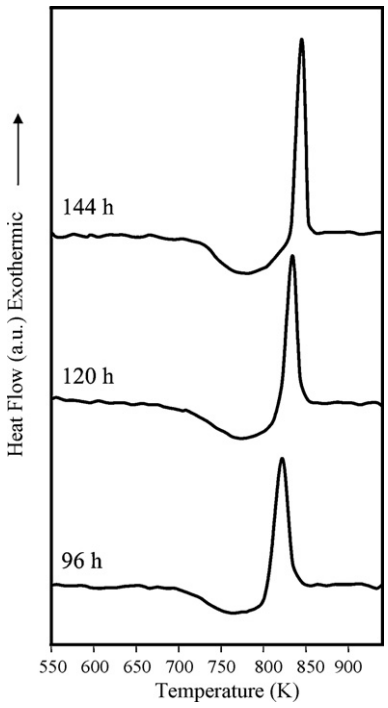

Fig. 3. DSC profiles of the amorphous samples.

milling times the particles have a higher uniformity and the shape of the particles becomes rounded. At the initial stages of the ball milling process (e.g. 6 h), due to the ball-powder-ball collisions, the high level of compressive forces were introduced into the powder particles and the particles obtained from this stage are the large agglomerated composite particles with a flattened morphology (Fig. 2(a)). The development of the MA process leads to a drastic fragmentation of the agglomerated particles and consequently the production of smaller particles with irregular shapes and a wide size distribution, as presented in Fig. 2(b). This phenomenon is attributed to the severe shear and impact forces applied to the powder particles during the high-energy ball milling process. After the sufficient milling time, the powder particles tend to reduce in size and show an irregular shape with a narrow size distribution (Fig. 2(c)). By further progression of the MA process, the homogeneity of the powders increases and the powder particles become regular in shape (Fig. 2(d)). Finally, the powder of the end-product (144 h) comprises homogeneous and smooth spheres with an average size of about 4 μm in diameter, as presented in Fig. 2(e). The last stage of the MA process in which all the particles are uniform in shape and in size signifies the completion of the solid state amorphization reaction [37].

3.3. Thermal studies

In order to investigate the structural variations of the as-milled amorphous powders (milling time ≥96 h) during the heat treatment process and to determine their glass-formation ability and crystallization behavior, differential scanning calorimetry (DSC) was conducted at a constant heating rate of 20 K/min (Fig. 3). The samples were heated up to 950 K (first run) and cooled down to about 400 K. Then, the second heating runs were performed to establish the base line. As it is obvious from Fig. 3, all of the samples reveal an endothermic event with a very large temperature span and a relatively sharp exothermic peak. With the purpose of determining the origin of these reactions, the DSC test was performed again on the as-milled samples in the same manner and the samples were heated up to the temperatures well below and above the temperature ranges of the reactions. Subsequently, the XRD analyses were performed on the samples at room temperature. Fig. 4 shows the XRD patterns of the samples milled for 144 h after the DSC test. The XRD profile of the samples taken before and after the endothermic event of the DSC curve does not show a significant structural change of the material, and no evidence of crystallization is found, whereas the samples annealed far above the exothermic reaction show the formation of the crystalline phases containing ferrite, CrN and Cr_2N. Accordingly, the endothermic reaction in the DSC curve reflects the heat capacity anomaly characteristic of the glass transition. Also, the exothermic peak indicates the succes-

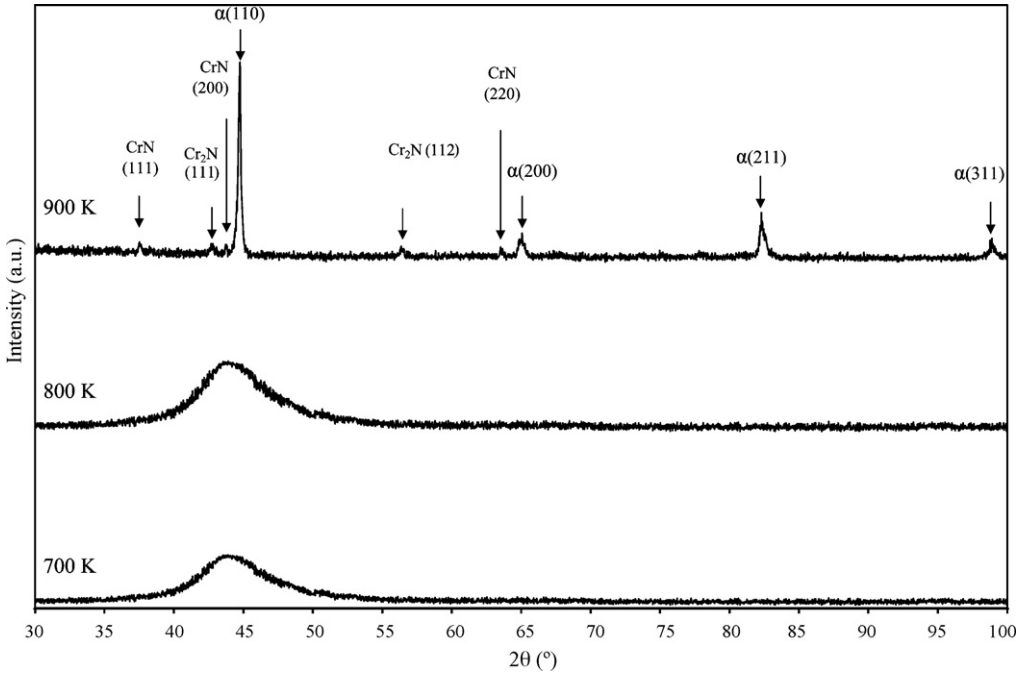

Fig. 4. XRD patterns of the samples milled for 144 h after the DSC test at 700, 800 and 900 K.

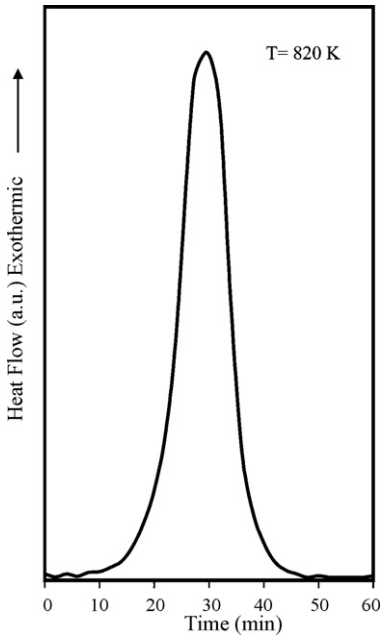

Fig. 5. Isothermal DSC test performed on the sample milled for 144 h.

sive stepwise transformation from a supercooled liquid state to the crystalline phases. Fig. 3 clearly signifies that as the milling time increases, the crystallization peak moves to higher temperatures, becoming more pronounced and sharp. This reveals that the quantity, homogeneity, and stability of the amorphous phase increase by increasing the milling time. The main contribution to these phenomena is the dissolved nitrogen atoms discussed by the authors in Ref. [35].

In order to increase the evidence of amorphicity, isothermal DSC scan was also conducted on the samples milled for 144 h (Fig. 5). The signals exhibit a typical bell shape for the first-order phase transition associated with the nucleation and growth. This confirms unambiguously that the high temperature exothermic events in Fig. 5 are related to the crystallization of the amorphous phase and not to the grain growth phenomenon of the nanocrystalline material.

Table 3 shows the exact amount of glass transition and crystallization temperatures, where T_g and T_x are the glass transition and onset crystallization temperatures, respectively. According to these data, the stability range of the supercooling liquid region (SLR) (T_x–T_g) increased by increasing the milling time, reaching 93 K for the samples milled for 144 h. There exist different aspects explaining this phenomenon. Inoue et al. [38] suggested that the large atomic size differences and the strong bonding nature between the constituent elements, along with the difficulty of the redistribution of these elements required for the crystallization are the dominant factors in the appearance of a wide SLR. With respect to the atomic radius of Fe (0.126 nm), Cr (0.128 nm) and Mn (0.127 nm), it can be concluded that in the absence of nitrogen, the first parameter (large atomic size ratios) is not an effective factor in the FeCrMn system. Furthermore, these three elements are close to each other in the periodic table and their heat of mixing is not considerable, revealing that the metallic bonding is not the main source of the wide SLR. Thus, the presence of nitrogen is essential to obtain the large SLR. It can be inferred that the appearance of the wide supercooled liquid region before crystallization is mainly due to the strong bonding energy between the constituent elements (especially chromium) and nitrogen, the difficulty of the atomic redistribution for the crystallization, and the requirement of large chemical fluctuations to form the critical nuclei of crystalline phases from the homogeneous amorphous phase.

Table 3
Quantity of T_g, T_x and SLR in the amorphous powders.

Milling time (h)	T_g (K)	T_x (K)	SLR (T_x–T_g) (K)
96	715	798	83
120	725	813	88
144	735	828	93

3.4. Magnetic studies

3.4.1. The as-milled samples

The magnetization vs. magnetic field properties were measured at room temperature for the as-milled powders and corresponding M–H loops are illustrated in Fig. 6. According to these results, the variation of saturation magnetization was shown in Fig. 7. According to these figures, the saturation magnetization decreases with increasing the milling time. This behavior could be explained by the following points:

(a) *Ferrite to austenite phase transformation*: ferritic stainless steels are usually classified as magnetic materials, whereas austenitic stainless steels are often described as non-magnetic, paramagnetic materials. At the initial stages of milling, the material consists of the major crystalline ferrite phase, providing a high saturation magnetization. By progression of MA, the ferrite phase disappears and the austenite phase begins to dominate and the saturation magnetization decreases.
(b) *Composition*: it is obvious that the saturation magnetization strongly depends on the composition. The saturation magnetization of a ferromagnetic material corresponds to the product of the net magnetic moment for each atom and the number of atoms in the material. The net magnetic moment of Fe atoms is considered to be larger than that of other atoms. With increasing the milling time by the nitrogen diffusion into the powder particles, the percentage of Fe for a given Fe18Cr12Mn composition decreases (Table 1), reducing the saturation magnetization. Furthermore, when the nitrogen atoms dissolve into the structure the interaction among the magnetic centers may reduce and the magnetic coupling may decrease, thereby decreasing the saturation magnetization.
(c) *Amorphous phase formation*: the decrease in the magnetization of the FeCrMnN alloys can result from their amorphous structure produced during the high-energy milling process. By progression of the MA process, an amorphous phase is created and grows along grain boundaries and consumes the crystalline lattice. At sufficiently milling times, the amorphization process is completed; consequently, the saturation magnetization decreases to 1.45 emu/g.

The coercivity of as-milled powders was also investigated by VSM. It should be mentioned that as the measurement of coercivity by VSM is inaccurate, to improve accuracy, before each measurement, an iron standard sample was used as a calibration sample. The variation of coercivity with milling time is indicated in Fig. 8. This variation could be discussed as follows:

(a) *Low milling times (<96 h)*: the coercivity increases as the milling time increases up to 96 h. This behavior could be explained by the following points:
  (1) It is obvious that the coercivity is in direct relation to the quantity of internal microstrain and defects. During MA under nitrogen atmosphere, due to the severe plastic deformation and incorporation of nitrogen into the structure, the

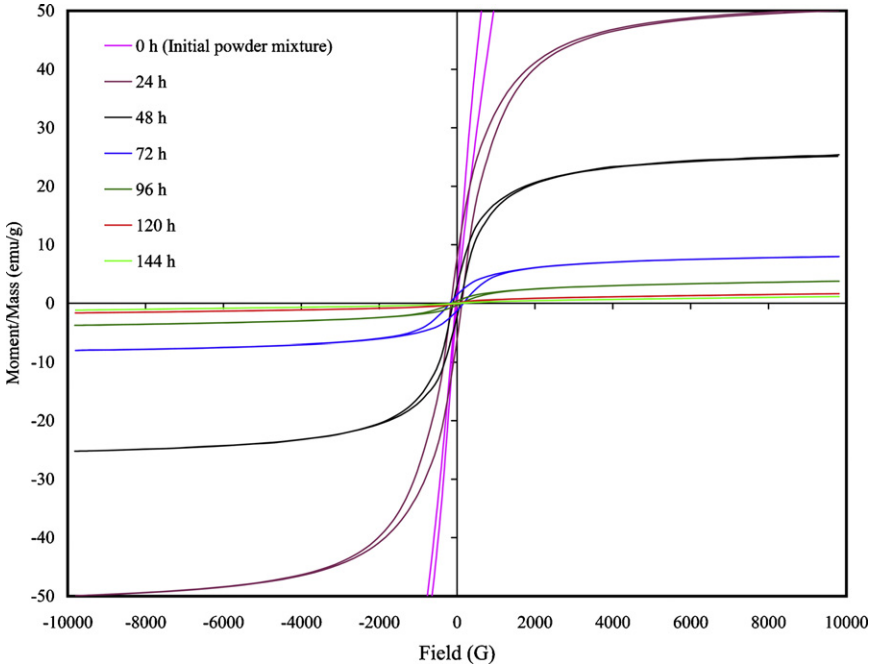

Fig. 6. Magnetization vs. magnetic field curve (M–H loop) of the as-milled samples.

amount of defect and lattice strain increases; therefore, the coercivity increases.

(2) Other factors affecting the coercivity are the crystallite size (D), saturation magnetization (M_s), and lattice parameter (a). The coercivity depends on these parameters as follows [39]:

$$H_c \approx 3\sqrt{\frac{kT_cK_1}{aM_s}}\frac{1}{D} \quad (1)$$

where H_c is the coercivity; K_1, the magnetocrystalline anisotropy; and T_c, the Curie temperature. According to the previous sections, by increasing the milling time, the quantity of D and M_s decreases and the value of a increases. As the variation of a with the milling time compared to D and M_s is considerably low, the effect of D and M_s on H_c is dominated over a and consequently the coercivity increases by progression of MA.

(3) The coercivity is in direct proportion to the volume percentage of non-magnetic phase (V_f) and in inverse relation to the saturation magnetization (M_s) as follows [40]:

$$H_c \propto \frac{\delta_w K_1}{M_s \mu_0 \bar{r}} V_f^{2/3} \quad (2)$$

where δ_w is the domain wall thickness; μ_0, the vacuum permeability; and $\bar{r}$, the average magnetic particle size. During the milling, due to the phase transformation of the magnetic ferrite phase to the non-magnetic austenite phase, the amount of non-magnetic phase (V_f) increases and consequently the coercivity increases. Furthermore, as discussed above, M_s decreases by progression of MA, thereby increasing the H_c according to Eq. (2).

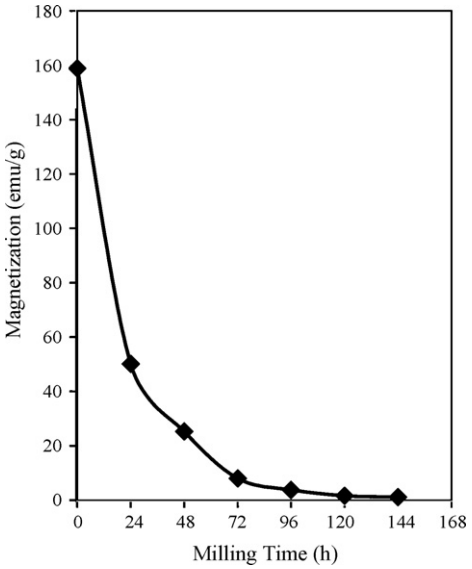

Fig. 7. The variation of saturation magnetization with milling time.

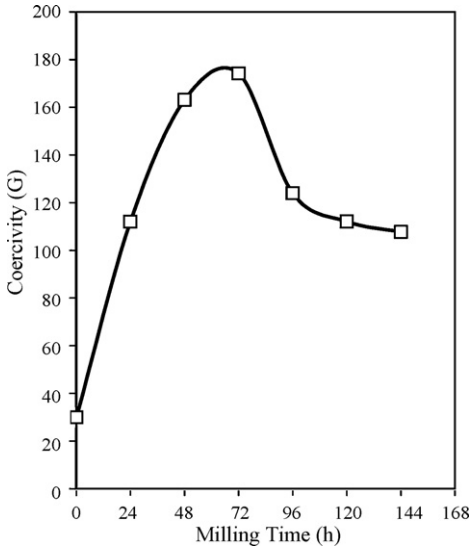

Fig. 8. The variation of coercivity with milling time.

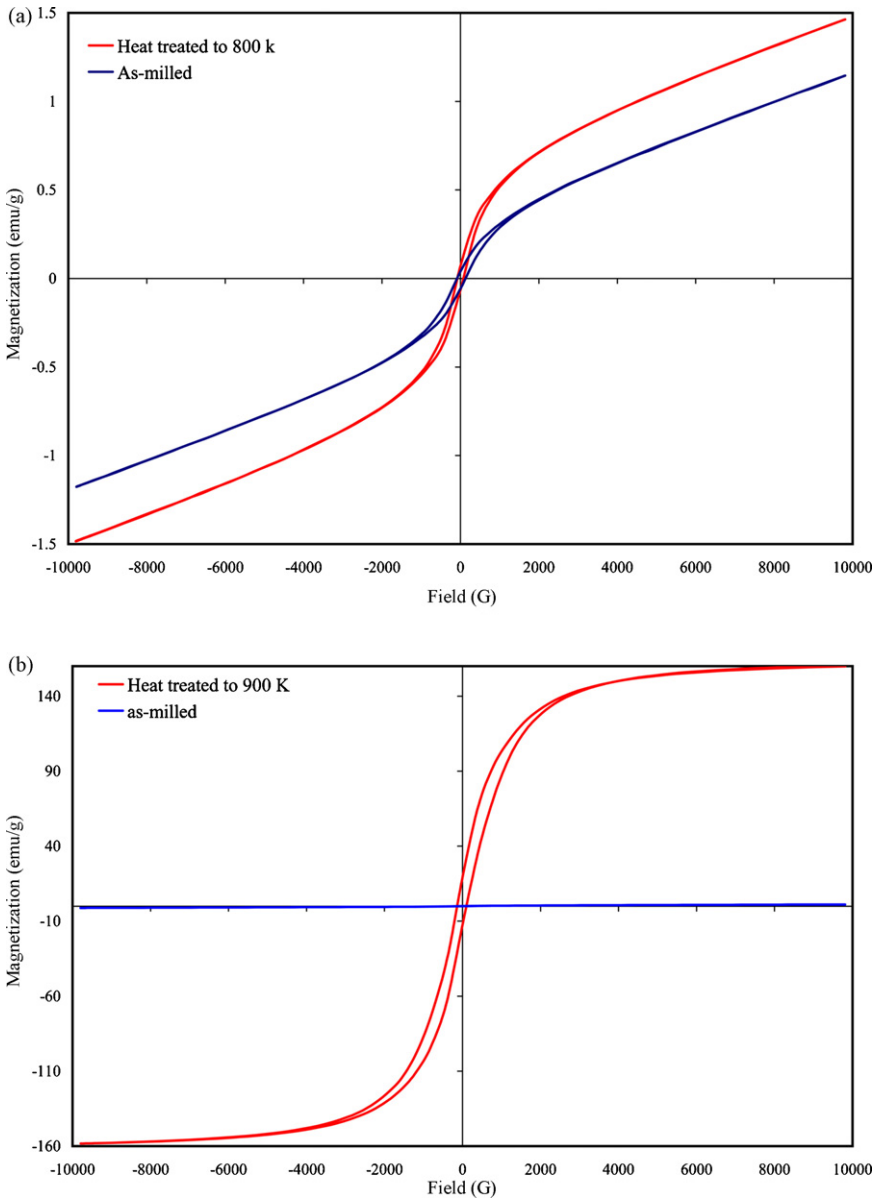

Fig. 9. Comparing the magnetization vs. magnetic field curves (M–H loop) of the samples milled for 144 h before and after heat treatment from room temperature to 800 K (a) and to 900 K (b).

(b) *High milling times (>96 h)*: the coercivity decreases as the milling time increases from 96 h to 144 h. It is well-established that for magnetic materials (in this case, the ferrite phase), lower than a special grain size, the coercivity follows the grain size with D^6 and decreases by decreasing the crystallite size [41,42]. Accordingly, in the present case, it can be inferred that the reduction of coercivity can be due to the reduction of the crystallite size of the crystalline ferrite phase, which may exist in small amounts in the structure, lower than the critical value and/or the formation of an amorphous phase from this magnetic phase.

3.5. The heat-treated samples

Fig. 9 demonstrates the effect of the heat treatment (DSC) on the magnetic properties of the sample milled for 144 h and compares the M–H loops of the sample before and after the DSC test. During the DSC test, the samples were heated up to 800 K (Fig. 9(a)) and 900 K (Fig. 9(b)) at a constant heating rate of 20 K/min. As it is obvious from Fig. 9(a), the saturation magnetization does not change considerably before and after the heat treatment. As discussed before (Fig. 4), after heating to 800 K, the structure does not change significantly and it contains a stress-free amorphous phase. Fig. 9(b) presents a noticeable increase in the saturation magnetization (MS) of the annealed samples. This increase can be due to the structural change and the nucleation of the nanocrystalline ferritic phase within the amorphous matrix.

According to the above-mentioned discussion, it can be inferred that by applying the suitable heat treatment process to the mechanically alloyed amorphous FeCrMnN alloys, the stress-free paramagnetic amorphous or ferromagnetic nanocrystalline alloys in the powder or bulk forms (after the consolidation of the powders) can be synthesized.

4. Conclusions

From this study, the following conclusions could be drawn:

(a) During milling under the nitrogen atmosphere, due to the solid–gas reaction, the high quantity of nitrogen atoms diffuses into the structure of the powders.
(b) A broad, diffuse and smooth halo appearing after 120 h of milling indicates the formation of a fully amorphous structure. This amorphous phase maintains its structure and is not transformed into other phases even after the longer milling times (144 h).
(c) The amorphous alloys exhibit two separate events in the DSC curves. The first endothermic peak is due to the glass transition reaction of the amorphous phase, whereas the second sharp exothermic peak is attributed to the crystallization of the amorphous phase.
(d) The amorphous alloys indicate a wide supercooled liquid region and their thermal stability increases by progression of MA due to the increase in their nitrogen concentration.
(e) According to the present experiment results, the magnetic coercivity increases and the saturation magnetization decreases with the time of milling. After completing the amorphization (>120 h), the material shows a paramagnetic behavior.
(f) The saturation magnetization of the amorphous powders does not change considerably by heating to temperatures well below the crystallization temperature. This allows for the production of bulk amorphous paramagnetic FeCrMnN alloys for potential technical applications, provided that the amorphous powders are compacted with suitable techniques.
(g) By applying the suitable heat treatment process to the amorphous powders, the amorphous phase is transformed to the nanocrystalline phases and the material depicts a considerable saturation magnetization. This allows for the production of bulk nanocrystalline ferromagnetic FeCrMnN alloys for scientific applications.

Acknowledgments

Shiraz University Research Council and Nanyang Technological University (NTU) are acknowledged due to their support for this study.

References

[1] H.S. Chen, Rep. Prog. Phys. 43 (1980) 353–432.
[2] P.Y. Lee, C.K. Lin, I.K. Jeng, C.C. Wang, G.S. Chen, Mater. Chem. Phys. 84 (2004) 358–362.
[3] X.Q. Zhang, E. Ma, J. Xu, J. Non-Cryst. Solids 352 (2006) 3985–3994.
[4] M. Seidel, J. Eckert, L. Schultz, Mater. Lett. 23 (1995) 299–304.
[5] H. Miura, S. Isa, K. Omuro, Jap. J. Appl. Phys. 29 (1990) L339–L342.
[6] H. Miura, K. Omuro, H. Ogawa, ISIJ Int. 36 (1996) 951–957.
[7] C.-J. Hu, P.-Y. Lee, Mater. Chem. Phys. 74 (2002) 13–18.
[8] K. Aoki, A. Memezawa, T. Masumoto, Appl. Phys. Lett. 1 (9) (1992) 1037–1039.
[9] P.P. Chattopadhyay, A. Samanta, W. Lojkowski, H.-J. Fecht, I. Manna, Metall. Mater. Trans. A 38A (2007) 2298–2307.
[10] H.M. Wu, C.J. Hu, H.C. Li, Formation of Co–Fe–M–B (M = Zr, Ti) amorphous powders by mechanical alloying and their magnetic properties, J. Alloys Compd. (2008), doi:10.1016/j.jallcom.2008.07.195.
[11] C. Suryanarayana, Prog. Mater. Sci. 46 (2001) 1–184.
[12] Y. Ogino, S. Murayama, Y. Yamazaki, J. Less-Common Met. 168 (1991) 221–235.
[13] Y. Ogino, T. Yamasaki, S. Murayama, R. Sakai, J. Non-Cryst. Solids 117–118 (1990) 737–740.
[14] T. Fukunaga, E. Ishikawa, T. Koyano, U. Mizutani, Physica B 213–214 (1995) 526–528.
[15] T. Fukunaga, N. Kuroda, C.H. Lee, T. Koyano, U. Mizutani, J. Non-Cryst. Solids 176 (1994) 98–103.
[16] K. Aoki, A. Memezawa, T. Masumoto, Mater. Sci. Eng. A181–182 (1994) 1263–1267.
[17] J.C. Rawers, D. Govier, R. Doan, Mater. Sci. Eng. A 220 (1996) 162–167.
[18] M. Méndez, H. Mancha, M.M. Cisneros, G. Mendoza, J.I. Escalante, H.F. López, Metall. Mater. Trans. A 33 (2002) 3273–3278.
[19] D. Shaham, J. Rawers, E. Zolotoyabko, Mater. Lett. 27 (1996) 41–45.
[20] A. Munitz, G. Kimmel, J.C. Rawers, R.J. Fields, Nanostruct. Mater. 8 (1997) 867–877.
[21] M.M. Cisneros, H.F. López, H. Mancha, D. Vázquez, E. Valdés, G. Mendoza, M. Méndez, Metall. Mater. Trans. A 33 (2002) 2139–2144.
[22] N. Nakada, N. Hirakawa, T. Tsuchiyama, S. Takaki, Script. Mater. 57 (2007) 153–156.
[23] M. Sumita, T. Hanawa, S.H. Teoh, Mater. Sci. Eng. C 24 (2004) 753–760.
[24] G. Balachandran, M.L. Bhatia, N.B. Ballal, P.K. Rao, ISIJ Int. 41 (2001) 1018–1027.
[25] S. Fréchard, A. Redjaïmia, E. Lach, A. Lichtenberger, Mater. Sci. Eng. A 480 (2008) 89–95.
[26] Z. Hua, Y.M. Sun, W.Q. Yu, M.B. Wei, L.H. Liu, Structure and magnetic properties of $Fe_{88-x}Zr_xB_{12}$ (x = 5, 10, 20) alloys prepared by mechanical alloying, J. Alloys Compd. (2008), doi:10.1016/j.jallcom.2008.10.075.
[27] M.D. Chermahini, S. Sharafi, H. Shokrollahi, M. Zandrahimi, Microstructural and magnetic properties of nanostructured Fe and $Fe_{50}Co_{50}$ powders prepared by mechanical alloying, J. Alloys Compd. (2008), doi:10.1016/j.jallcom.2008.06.144.
[28] M.P.C. Kalita, A. Perumal, A. Srinivasan, J. Magn. Magn. Mater. 320 (2008) 2780–2783.
[29] Y.J. Liu, I.T.H. Chang, M.R. Lees, Mater. Sci. Eng. A 304–306 (2001) 992–996.
[30] N. Sulitanu, Mater. Sci. Eng. B 90 (2002) 163–170.
[31] H.R. Madaah Hosseini, A. Bahrami, Mater. Sci. Eng. B 123 (2005) 74–79.
[32] G.N. Konygin, E.P. Yelsukov, V.E. Porsev, J. Magn. Magn. Mater. 288 (2005) 27–36.
[33] S. Xu, M. Zhong, L. Yu, H. Chen, Z. He, J. Zhang, J. Magn. Magn. Mater. 303 (2006) 73–78.
[34] E.P. Yelsukov, G.A. Dorofeev, A.V. Zagainov, N.F. Vildanova, A.N. Maratkanova, Mater. Sci. Eng. A 369 (2004) 16–22.
[35] R. Amini, M.J. Hadianfard, E. Salahinejad, M. Marasi, T. Sritharan, J. Mater. Sci. 44 (2009) 136–148.
[36] R. Amini, M.J. Hadianfard, E. Salahinejad, M. Marasi, T.Sritharan, J. Non-Cryst. Solids, in press.
[37] M. Sherif El-Eskandarany, A.A. Bahgat, N.S. Gomaa, N.A. Eissa, J. Alloys Compd. 290 (1999) 181–190.
[38] A. Inoue, T. Zhang, T. Masumoto, J. Non-Cryst. Solids 156–158 (1993) 473–480.
[39] R. Koohkan, S. Sharafi, H. Shokrollahi, K. Janghorban, J. Magn. Magn. Mater. 320 (2008) 1089–1094.
[40] C.W. Chen, Magnetism and Metallurgy of Soft Magnetic Materials, Dover publications, New York, 1980.
[41] M.E. McHenry, M.A. Willard, Prog. Mater. Sci. 44 (1999) 291–433.
[42] E. Kita, N. Tsukuhara, H. Sato, K. Ota, Hi. Yangaihara, Appl. Phys. Lett. 88 (2006) 152501-1–152501-3.